(SN) 2133

New Sources for Real Applications in the Far Infrared

H. N. Rutt, Zhi-Jun Xin
Optoelectronics Research Centre
University of Southampton, Highfield, Southampton SO17 1BJ, UK

SUMMARY - *Novel multiple quantum well structures for use as the active elements in optically pumped far infrared lasers are proposed. Optimization of the quantum well design and the effect of growth tolerences are investigated. A surface-loaded waveguide structure is proposed for mode control.*

1 Introduction

The far infrared (FIR) is something of a "Cinderella" region where, aside from some molecular spectroscopy, astronomy and solid state physics rather little work is carried out - and virtually no real world applications. The meaning of 'far infrared' is not even very well defined, but we take it to be the region from 25um to 500um in wavelength. Below 25um the vibrational transition lasers and applications based on vibrational spectroscopy are well established. Above 500um in the sub millimetre region radio frequency techniques can be applied. However the far infrared, over a decade in bandwidth, sees little exploitation. The poor performance of uncooled or 77K detectors in this region is of fundamental origin, so progress depends on practical FIR sources. Current FIR lasers are either free electron lasers which are excellent research tools but impractical for general use, and pure rotational transition gas lasers. These are large and place stringent conditions on the carbon dioxide laser needed to pump them, and are impractical in most applications.

A great deal of work has been done on the feasibility of optically induced FIR emission from the intersubband transition in QW structures [1-9]. Intensive research has been done on the double-well [9-12] structures. FIR emission has been observed from the double-well structure. Evidence in [13] shows that population inversion has been achieved in the stepped-well.

For conventional lasers, there are two schemes. One is the 4-level system represented by Nd^{3+}:YAG and the other is 3-level system like a ruby laser. Generally, the 4-level system has advantages in lasing threshold, efficiency and duty cycle over the 3-level system. Two optically pumped FIR QW lasers are proposed, a four and a three level structure analogous to the conventional laser systems. However it should be noticed that the three level scheme considered is one in which the pump and laser transition share a common upper level (analogous to optically pumped FIR gas lasers) as opposed to a common lower level, as is the case for a ruby laser. This scheme has far lower thresholds and potential for CW laser action as compared to the "ruby" arrangement, owing to the low lower level population.

Three and four-level schemes are compared and we improve the structures with regard to gain and hence predicted threshold pump power. The QWs and the shapes of the structures have been carefully tailored to optimize them in terms of the oscillator strengths, nonradiative rates, waveguide efficiencies and gains. We consider the effects of growth tolerances on the realization of such lasers.

2 Transitions

In a QW laser, the radiative and non-radiative transition rates determine the emission efficiency. These are proportional to the overlap between the wavefunctions involved in the transitions [7]. Therefore we start our optimization by engineering the QW so that it favours the radiative transition and suppresses the non-radiative transition.

In GaAs, when the subband gaps is greater than 36 meV, the major scattering mechanism resulting in nonradiative transitions is interaction with the polar longitudinal optical (LO) phonons, while when the energy separation is significantly lower than 36meV, it is dominated by interaction with the acoustic phonons and the transition rate is about two orders of magnitude lower [7]. The transition rate can be calculated by

AITA-Advanced Infrared Technology and Applications-Venezia 1999, pp.25-33

the golden rule formula from the initial state $|i\rangle$ with energy E_i to the final state $|f\rangle$ with energy E_f caused by a scatterer H' with emission or absorption of a quanta $\hbar\omega_q$:

$$W_{if} = \frac{2\pi}{\hbar}|\langle f|H'|i\rangle|^2\delta(E_i - E_f \mp \hbar\omega_q) \tag{1}$$

where the "$\mp$" in the δ function takes "$-$" for absorption and "$+$" for emission. For LO phonon emission $\omega_q = \omega_{LO} = 36\text{meV}$, $H' = \sum_{\vec{q}}[\alpha(\vec{q})\exp(-i\vec{q}\cdot\vec{r})b^\dagger_{\vec{q}}]$, where $b^\dagger_{\vec{q}}$ is the creation operator for a LO phonon in mode $\vec{q}$ and $\alpha(\vec{q})$ is the electron phonon interaction.

$$|\alpha(\vec{q})|^2 = 2\pi\hbar\omega_{LO}\frac{e^2q^2}{V(q^2+q_s^2)^2}\left(\frac{1}{\epsilon_\infty} - \frac{1}{\epsilon_s}\right) \tag{2}$$

where q_s is the inverse of the 3D screening length (q_s is taken as 0 in this paper), ϵ_s and ϵ_∞ are the static and high frequency permittivities. For photon absorption or emission, $H' = \sqrt{\hbar(n_{ph}+int)/2\omega\epsilon}\, a\cdot\nabla$, where $int = 0$ for absorption and $int = 1$ for phonon emission, n_{ph} is the photon density in the initial state, ϵ is the dielectric constant and a the polarization unit vector of the photons.

In the above equations, in order to optimize the performance of a FIR QW laser we must shape the subbands in such a way that the electrons involved in the pumping and lasing transitions have a maximum interaction with photons while their interaction with phonons is minimized. Ideally the overlap of the subbands $|i\rangle$ and $|f\rangle$ in the momentum matrix element $\langle f|H'|i\rangle$ of the radiative transition is maximized so that the pumping and lasing efficiencies are as large as possible. Because the photo-excited electrons in $|f\rangle$ can also make the reverse transitions to $|i\rangle$ by interaction with phonons, the nonradiative transition rates should be kept low in the optimization. If we assume that the electrons are pumped from the ground subband G to F and lase from l to l', then we also require that the populating process from F to l is faster than the depopulating process from l' to G so that CW FIR laser action is possible.

Based on the above considerations, we obtain two designs from GaAs-$Al_xGa_{1-x}As$ QW system as shown in figure 1. One is stepped in shape and the other is a parallel QW structure. The parameters defining

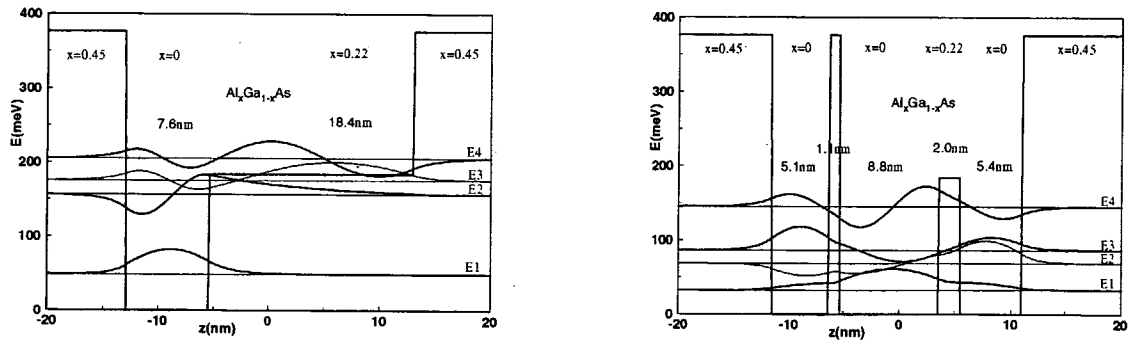

Figure 1: The subbands and wavefunctions at $\vec{k} = 0$ in the stepped and parallel QWs.

the QW structures were manually adjusted to empirically minimize the lasing threshold (Section 4). In the designs, the maximum composition for the direct band is used, $x = 0.45$ so as to increase the quantum confinement, hence increasing the wavefunction overlap in the QW. In the stepped QW a deep side-placed narrow well combined with a shallow wide well maximizes the asymmetric effect which greatly increase the strength of the optical transition from E_1 to E_3. In the parallel QWs, two internal barriers are used for the same purpose. The wavefunctions for E_1 in the two designs are mainly confined in the narrow well so that their transition rates can be high both for pumping (E_1 to E_3 for the stepped QW or E_1 to E_4 for the parallel QWs) and depopulating processes (E_2 to E_1) but relatively low for the nonradiative transition from E_3 to E_1 in the stepped QW or from E_4 to E_1 in the parallel QWs. The energy gaps for the lasing transition are designed to be $\Delta E_{32} < 36\text{meV}$, so that the nonradiative transition is suppressed. The pump energy $\Delta E_{GF} \sim 117\text{meV}$ has been set in the tunable CO_2 laser wavelength range.

The stepped QW is similar to a typical three level scheme such as a carbon dioxide laser pumped FIR gas laser. The parameters are listed in table 1. Photon absorption and emission are proportional to the oscillator strength f . The oscillator strengths related to the pump and lasing transitions are given in the third column. The subband energy levels E_i and the scattering rates W_{ij} caused by LO phonons are also

calculated. Here $\Delta E_{32} = 19\text{meV}$ is less than the LO phonon energy 36meV, so the nonradiative scattering for the transition is mainly caused by the acoustic phonon which is $W_{32} \sim 1 \times 10^{10}\text{s}^{-1}$ much lower than W_{31} and W_{21}. The electrons in E_1 are pumped by a CO_2 laser to E_3. Since $W_{31} < W_{21}$, we can expect population inversion between E_3 and E_2.

The three parallel QW structure works in a similar way to typical optically pumped four-level lasers. The calculated subbands, LO phonon scattering rates and related oscillator strengths are listed in table 2.

For comparison with our designs, using the parameters provided in [8], we also calculated the subband levels, LO phonon emission rates and the oscillator strengths of the stepped QW in [8], see table 3. The E_1 to E_5 pump transition was used in the design to suit the CO_2 laser wavelength and f_{15} for the transition was found to be very small, which implies a very low pump absorption coefficient.

3 Waveguide

Since the active layer is very thin and the oscillator strength for the pump transition is weak, the pump and lasing light must be waveguided and effectively overlapped with the active layer. A fundamental difficulty arises in that the large ratio of lasing wavelength λ_l and pump wavelength λ_p implies that for a simple guide even a single mode guide at λ_l will be highly multi-mode at λ_p. In this situation it is difficult to guarantee good mode overlap unless a chosen high order mode of good overlap can be launched, which is difficult in practice. To realize a waveguide at $\lambda_p = 10.6\mu\text{m}$ for pump light, we suggest that a germanium layer is deposited on the top of the capping layer so that both the pump and lasing beams can be well confined in the active region.

Figure 2 shows the overall structures for the two designs. The thick rectangular lines in the two diagrams give the layer refractive indexes.

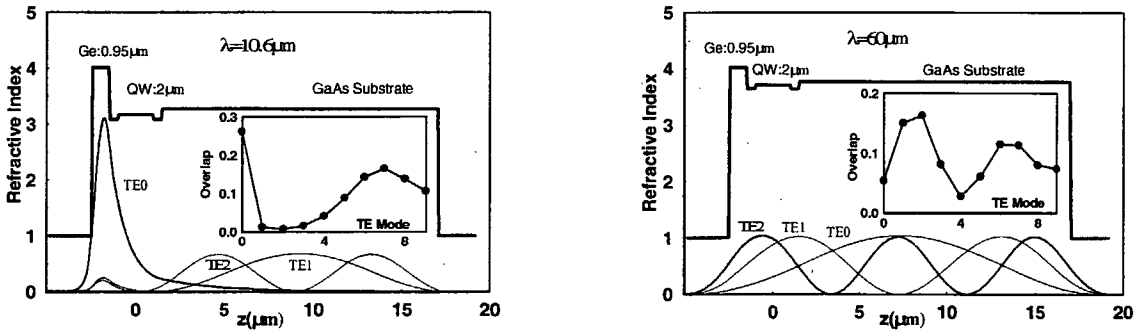

Figure 2: The intensity distribution of the pump light and the lasing light in a cross-section of the QW structures and their overlaps with the QW layer.

Also shown in figure 2 are the intensity (arbitrary units) variations of the pump and laser modes in a cross-section. With an $0.95\mu\text{m}$ germanium cladding layer, the TEM_{00} mode (thick line) of pump light has been strongly confined in the germanium layer but has good overlap with the QW active layer where the electrons are pumped. The inset is the variation of the overlap ratios in the QW active layer for different TE modes. Also shown in the lower is the waveguide TE modes for the lasing modes. The overlap of the lasing mode with the germanium layer is small, so that its loss is not critical. The germanium layer serves a purely optical function and is not required to be epitaxially grown, so that it may be deposited by any

Table 1: Calculated data on the stepped quantum wells.

Subbands(meV)	Emission Rate(s^{-1})	Oscillator Strength
$E_1 = 48.53$	$W_{31} = 0.201 \times 10^{12}$	$f_{13} = 0.100$
$E_2 = 156.5$	$W_{21} = 1.383 \times 10^{12}$	$f_{32} = 0.677$
$E_3 = 175.5$		

Table 2: Calculated data on the parallel quantum wells.

Subbands(meV)	Emission Rate(s^{-1})	Oscillator Strength
$E_1 = 32.3$	$W_{43} = 5.33 \times 10^{12}$	$f_{14} = 0.17$
$E_2 = 68.3$	$W_{42} = 4.40 \times 10^{12}$	$f_{32} = 1.18$
$E_3 = 86.0$	$W_{41} = 2.12 \times 10^{12}$	
$E_4 = 145.0$	$W_{31} = 3.20 \times 10^{12}$	
	$W_{21} = 6.59 \times 10^{12}$	

Table 3: Calculated results on the stepped quantum well based on the parameters of Afzali-Kushaa et al.

Subbands(meV)	Emission Rate(s^{-1})	Oscillator Strength
$E_1 = 17.3$	$W_{53} = 3.97 \times 10^{12}$	$f_{15} = 9.75 \times 10^{-4}$
$E_2 = 58.4$	$W_{52} = 2.45 \times 10^{12}$	$f_{14} = 7.87 \times 10^{-4}$
$E_3 = 79.8$	$W_{51} = 0.26 \times 10^{12}$	$f_{31} = 2.32 \times 10^{-2}$
$E_4 = 101.3$	$W_{31} = 1.02 \times 10^{12}$	$f_{32} = 1.18$
$E_5 = 120$	$W_{21} = 6.28 \times 10^{12}$	

conventional method such as sputtering. The substrate is thinned to reduce the loss outside the QW layer and improve the overlap and thermal conduction.

4 Gain

For a GaAs parabolic conduction band, the optical gain for the radiative transition between subbands in a QW is given by [8, 14]

$$g(\omega) = \frac{\pi c^2 \Delta n_s}{d\varepsilon_r \tau_e \omega^2} \frac{T_2}{1 + (\omega - \omega_0)^2 T_2^2}. \tag{3}$$

where Δn_s is the population inversion sheet density between the lasing subbands, d is the thickness of the QW layer, $\omega = \delta E/\hbar = 2\pi c/\lambda$ is the angular frequency and ω_0 is the resonant angular frequency, ε_r is the relative permittivity of GaAs, T_2 is the dephasing time of lasing subband E_3 and τ_e is the spontaneous radiative time. The threshold gain at the resonant frequency is obtained when the optical gain in equation 3 equals the absorption losses α_{qw} in the QW region and α_{ph} in the intrinsic region of the cladding layers and the reflective loss.

$$\frac{d}{t_m} g_{th} = \frac{d}{t_m} \alpha_{qw} + \frac{t_{cl}}{t_m} \alpha_{ph} + \frac{1}{L} \ln\left(\frac{1}{R}\right) \tag{4}$$

where $t_m = \lambda/2\sqrt{\varepsilon_r}$ is effective mode thickness, t_{cl} is the thickness of the cladding layers, L is the laser cavity length and R is the mirror reflectivity. The population change at subband i resulting from photon and phonon scattering can be expressed as

$$\frac{dn_i}{dt} = N_p \delta(i - F) + \sum_{j>i} W_{ji} n_j - N_p \delta(i - 1) - n_i \sum_{j<i} W_{ij} \tag{5}$$

where N_p is the pump rate of the electrons into subband F (F is 4 for the 4-subband parallel QW system and 3 for the 3-subband stepped QW system). At equilibrium, dn_i/dt is zero. The population inversion is $\Delta n = n_3 - n_2$, so for a 3-subband system

$$\Delta n_s = N_p \frac{W_{21} - W_{32}}{W_{21} W_{32} + W_{21} W_{31}} \tag{6}$$

and for a 4-subband system

$$\Delta n_s = N_p \frac{W_{21} W_{43} - W_{42} W_{32} - W_{42} W_{31} - W_{32} W_{43}}{(W_{21} W_{32} + W_{21} W_{31})(W_{43} + W_{42} + W_{41})} \tag{7}$$

W_{ij} can be obtained from equation 1. For the 3-subband system, an electron in E_F can only transit to the ground E_1 via the routes $E_3 \rightarrow E_1$ or $E_3 \rightarrow E_2 \rightarrow E_1$. However for the 4-subband system it can be via either $E_4 \rightarrow E_1$ or $E_4 \rightarrow E_2 \rightarrow E_1$, $E_4 \rightarrow E_3 \rightarrow E_1$ and $E_4 \rightarrow E_3 \rightarrow E_2 \rightarrow E_1$. Only the route containing the transition W_{32} contributes to the FIR emission. For the designs in figure 1 the pump efficiency $\Delta n_s/N_p$ in the 3-subband system is 1.8×10^2 higher than that in the 4-subband system.

In equation 4 the absorption loss α_{qw} in the QW is zero because plasmon oscillations of the electrons in the QW can only coupled to radiation polarized parallel to the QW layer while the IR emission arising from the intersubband transition is polarized perpendicularly to the QW layer [14, 7]. Because the germanium layer is intrinsic and the free carrier concentration is low at low temperature and the FIR mode overlap with it is small, the loss α_{cl} due to free carrier absorption in the region is negligible. The threshold pump power intensity required for lasing can be then written as $I_{th} = N_p\hbar\omega/\eta\Gamma$, where η is the overall quantum yield for the pump light and Γ is the product of the overlap ratios Γ_p and Γ_l of the pump and laser modes with the QW layer. Γ_p is constant for a pump wavelength of 10.6μm. Taking mirror reflectivity $R = 0.3$ (cleaved facets), $L = 1$mm, $\eta = 0.15$, $T_2 = 0.21$ps and substituting the quantities in equation 6, 7 and I_{th} with the optimized data obtained in Section 3 and 4, we can draw in figure 3 the variation of the threshold pump power intensity against lasing wavelength for 50 QWs of the 3 and 4-level structures. A constant Γ_l at $\lambda = 60\mu$m has been used in the calculation though it will become smaller at a longer wavelength causing a rise in threshold. The emission wavelength at the short side is limited to $\sim 50\mu$m by the LO scattering. However there seems no limitation at the long wavelength side provided the wavelength remains above cut-off at λ_l. Increasing the thickness can increase the cut-on wavelength. On the other hand however, it also brings

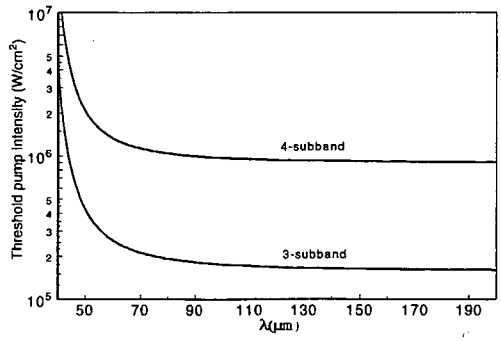

Figure 3: The threshold pumping (CO_2 laser at 10.6μm) power intensity vs the emission wavelength for 50 QWs.

problems with overlap, thermal dissipation and free carrier absorption.

In equation 5 we have ignored thermal effect on population. At room temperature, $\Delta E_2 = 156.5$meV for the 3-subband system is much higher than the corresponding thermal energy 26meV; while $\Delta E_2 = 68$meV for the 4-subband system is comparable to 26meV. For a sheet density $n_s = 1 \times 10^{11}/\text{cm}^2$, the Fermi energy level is at $\sim$ 31meV below E_1. So the electrons are significantly thermally excited to E_2 for the 4-subband system. This will require even higher threshold pump intensity for the 4-subband system, unless operated at very low temperatures.

5 Effect of Growth Tolerances

In practice, many factors, such as molecular beam flux, pressure, temperature etc. in MBE or MOCVD growth, can give rise to inhomogeneity of the QW structures owing to time fluctuation and spatial non-uniform distribution of the factors during growth of multi-QW structures. In [15], we discussed the inhomogeneities arising from systematic drift and gaussian random deviation. Here we discuss the influence of the inhomogeneities on the lineshape and gain.

The distribution function of gain intensity over ω can be expressed as [15]:

$$g_{g,l}(\omega, \omega_0) = \frac{\pi c^2 p_{g,l}(\omega_0)\Delta n_s}{d\varepsilon_r \tau_e \omega^2} \frac{T_2}{1 + (\omega - \omega_0)^2 T_2^2} \tag{8}$$

where the second factor is the Lorentzian lineshape factor of a single QW, Δn_s the population inversion sheet density between the lasing subbands in a QW, d the thickness of the QW, $\omega = \Delta E/\hbar = 2\pi c/\lambda$ the angular frequency and ω_0 the resonant angular frequency, ε_r the relative permittivity of the system, $\Delta\omega = 2/T_2$ the full-half-width of the spontaneous emission and T_2 the dephasing time of the spontaneous emission, $\tau_e \propto \omega^{-2}$ the lifetime of the spontaneous emission and p_g and p_l gaussian and uniform distribution functions of the QWs at frequency ω_0 respectively.

For a very large scale fluctuation and a limited number of QWs (in our case this number is normally less than 50), it is very hard to establish a statistical model to approximate the fluctuation. Fortunately for mature MBE growth and GaAs systems, the fluctuation can be controlled to a small to intermediate scale, a few monolayers and a few percent of mole fraction [16]. In this case, the scatter of the structural parameters of multi-QW systems caused by growth factor fluctuations can be approximated by a gaussian or uniform distribution function:

$$\begin{aligned} p_g(\omega_0) &= \frac{N}{\sqrt{2\pi\sigma^2}} \exp\left[-\frac{(\omega_c-\omega_0)^2}{2\sigma^2}\right], \\ p_l(\omega_0) &= \frac{N}{(\omega_h-\omega_l)}. \end{aligned} \tag{9}$$

where $p_g(\omega_0)$ and $p_l(\omega_0)$ represent a gaussian and uniformly distributed models respectively, σ is the standard deviation of ω_0 from the centre frequency ω_c, for the uniform distribution, $\sigma = (\omega_h - \omega_l)/\sqrt{12}$ and $\omega_c = (\omega_h + \omega_l)/2$ and ω_l and ω_h are the extrema of the frequency drift range. $p_g(\omega_0)$ and $p_l(\omega_0)$ are normalized in the range $0 \le \omega_0 \le \Delta E_c/\hbar$ and $\omega_l \le \omega_0 \le \omega_h$ respectively, where ΔE_c is the conduction band offset in the QW lasers. Here for the $p_l(\omega_0)$, distribution caused by the systematic deviation we take only the case of uniform distribution because it represents the worst fluctuation of this kind [15].

When $\omega = \omega_0$ Equation 8 represents the magnitude of the gain intensities at different resonant frequencies ω_0:

$$g_{m(g,l)}(\omega_0) = \frac{\pi c^2 \Delta n_s T_2}{d\varepsilon_r \tau_e \omega_0^2} p_{g,l}(\omega_0) \tag{10}$$

So $g_{m(g,l)}(\omega_0)$ varies proportionally with $p_{g,l}$ and g_{mg} has maximum at $\omega_0 = \omega_c$.

For a given ω, g_g or g_l describes the spectral intensity of gain at ω for different QW layers with different resonant frequencies ω_0. The integration of $g_g(\omega,\omega_0)$ or $g_l(\omega,\omega_0)$ over ω_0 in the resonant frequency range gives the total gain at frequency ω:

$$\begin{aligned} G_g(\omega) &= \int_{-\infty}^{\infty} g_g(\omega,\omega_0)d\omega_0, \\ G_l(\omega) &= \int_{\omega_l}^{\omega_h} g_l(\omega,\omega_0)d\omega_0. \end{aligned} \tag{11}$$

Here for convenience of calculation, the integration range for $G_g(\omega)$ is changed from $0 \le \omega_0 \le \Delta E_c/\hbar$ to $-\infty < \omega_0 < \infty$ because for small to intermediate scale inhomogeneity of a monolayer or two, out of the range $0 \le \omega_0 \le \Delta E_c/\hbar$, g_g is very small and this change only introduces a negligible error. Hence $G_g(\omega)$ or $G_l(\omega)$ gives not only the gain spectral distribution but also the lineshape of QW lasers under gaussian fluctuations or systematic drift of the well parameters.

By substituting $(\omega_c - \omega_0)$ with ω_0' and considering the maximum gain at $\omega = \omega_c$, we can obtain the total gains of G_g and G_l at the central frequency ω_c and see their dependence on the broadening factors σ and T_2. In other words, this shows the relationship of the maximum gain with the lineshape parameters σ and T_2.

$$\begin{aligned} G_g(\omega_c) &= \int_{-\infty}^{\infty} \frac{\pi c^2 \Delta n_s}{d\varepsilon_r \tau_e \omega^2} \frac{N}{\sqrt{2\pi\sigma^2}} \exp\left(-\frac{\omega_0'^2}{2\sigma^2}\right) \frac{T_2}{1+\omega_0'^2 T_2^2} d\omega_0' \\ &= \frac{\pi c^2 \Delta n_s N}{d\varepsilon_r \tau_e \omega^2 \sigma} \sqrt{\frac{\pi}{2}} \exp\left(\frac{1}{2\sigma^2 T_2^2}\right) \left[1 - \operatorname{erf}\left(\sqrt{\frac{1}{2\sigma^2 T_2^2}}\right)\right] \\ G_l(\omega_c) &= \int_{\omega_l}^{\omega_h} \frac{\pi c^2 \Delta n_s}{d\varepsilon_r \tau_e \omega^2} \frac{N}{\omega_h - \omega_l} \frac{T_2}{1+\omega_0'^2 T_2^2} d\omega_0' \\ &= \frac{\pi c^2 \Delta n_s N}{d\varepsilon_r \tau_e \omega^2 \sigma} \frac{1}{\sqrt{3}} \arctan\left(3\sigma^2 T_2^2\right) \end{aligned} \tag{12}$$

In the equations, the first term is independent of ω since $\tau_e \propto \omega^{-2}$. The gain intensity in the integrations consists of two parts which have an effect on the lineshape: one is the QW distribution and the other is the Lorentzian broadening. The gains for the two distributions are inversely proportional to σ. This means that any inhomogeneity introduced in growth will directly result in gain reduction and its effect on the gain is inversely proportional to its fluctuation. When T_2 is finite but $\sigma \to 0$ in p_g and p_l, p_g and p_l approach the Dirac function $N\delta(\omega_c - \omega_0)$. This is the situation in which the inhomogeneity is negligible. In this case the integration results of G_g and G_l have a similar form to that in Equation 8, except for that $p_g\Delta n_s$ and $p_l\Delta n_s$ become $N\Delta n_s$, and the line widths of G_g and G_l are determined by the Lorentzian broadening, $2/T_2$. The variation of G_g and G_l with respect to σT_2 can be seen more explicitly in Figure 4, along with them are the gain G_0 for a uniform QW structure and G_∞, where

$$G_\infty = \frac{\pi c^2 N \Delta n_s}{d\varepsilon_r \tau_e \omega^2} \frac{1}{\sigma}. \tag{13}$$

In order to present a result of general relevance, the gains G_g, G_l and G_∞ have been normalized to G_0. As can be seen, G_g, G_l approach G_0 when $\sigma T_2 \to 0$, but they rapidly decrease and get close to G_∞ when $\sigma T_2 \gg 1$, and for the same σT_2, G_g is always greater than G_l. In Figure 4 T_2 is taken as a constant and σ varies. However the same limiting properties of G_g and G_l apply when σ is finite but T_2 changes to the extremes, because of the symmetry of σ and T_2 in Equation 12.

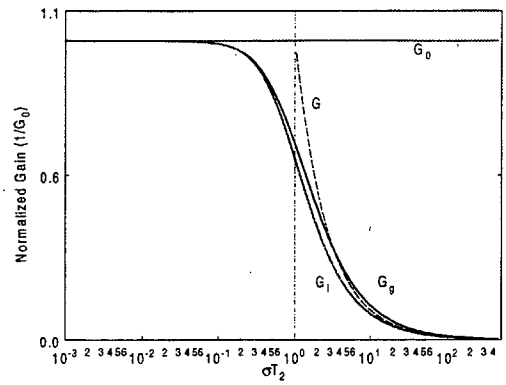

Figure 4: When T_2 is finite, the dependence of normalized gains G_g and G_l on σT_2, along with them are G_0 and G_∞ to compare the approach properties when $\sigma \to 0$ and $\sigma \to \infty$. The same approaches can be obtained when σ is finite but T_2 changes. The gain decrease due to the inhomogeneity can be seen by comparison of G_g and G_l with G_0.

The variation of linewidth with σ is also an important technological parameter, but in contrast to the peak gain no closed form expression has been found for this, and we present numerical results. Figure 5 shows the variation of the full-half-widths of G_g and G_l with σT_2 after being normalized to $2/T_2$. As in the Figure 4, T_2 is taken as a constant and σ varies. As can be seen, for small σT_2 the change of the line widths of G_g and G_l are approximately equal to $2\sigma + 2/T_2$ or $2/T_2$. However for $\sigma \to \infty$, the full-half-widths approaches 2σ and the full-half-width for gaussian distribution is smaller than that for uniform distribution. The line broadening due to the inhomogeneity can be seen by comparison of curves of the full-half-width with the line of $2/T_2$.

6 Conclusion

We have presented detailed designs for optically pumped far infrared lasers based on multiple quantum well structures pumped by a CO_2 laser. A three-level device proves optimum , and the tolerances required are feasible. A top loaded waveguide structure employing a germanium layer is proposed for mode control. There appears excellent prospects for the operation of this new FIR source.

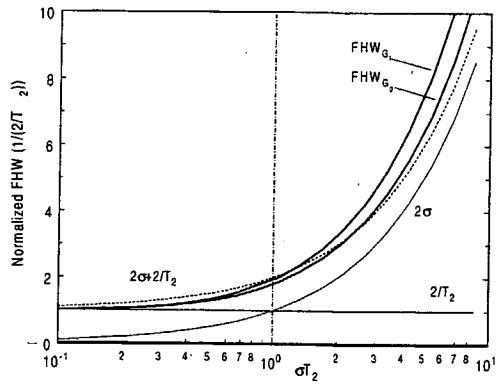

Figure 5: The normalized full-half-widths (bold curves) of gains for gaussian and uniform distributions as a function of the inhomogeneous fluctuation σ. Also shown are the homogeneous broadening due to momentum scattering $2/T_2$, the inhomogeneous broadening due to structural fluctuation 2σ and their sum $2(\sigma + T_2)$ (dotted curve). The line broadening due to the inhomogeneity can be seen by comparison of the curve of the full-half-width with the line of $2/T_2$.

Acknowledgement

The authors thank Engineering and Physical Science Research Council (EPSRC) for financial support and the EPSRC III-V Semiconductor Central Facility for useful discussion over MBE growth fluctuation.

References

[1] M. Helm, E. Colas, P. England, F. DeRosa, and S. J. Allen Jr. "Observation of grating-induced intersubband emission from GaAs/AlGaAs superlattices". *Appl. Phys. Lett.*, 53(18):1714–1716, 1988.

[2] Kei May Lau and Wei Xu. "Optically pumped submillimeter wave semiconductor lasers". *IEEE J. Quantum Electronics*, 28(8):1773–1777, 1992.

[3] A. Kastalsky. "Infrared intraband laser induced in a multiple-quantum-well interband laser". *IEEE J. Quantum Electronics*, 29(4):1112–1115, 1993.

[4] Gang Sun and Jacob B. Khurgin. "Optically pumped four-level infrared laser based on intersubband transitions in multiple quantum wells: feasibility study". *IEEE J. Quantum Electronics*, 29(4):1104–1111, 1993.

[5] C. Sirtori, F. Capasso, J. Faist, L. N. Pfeiffer, and K. W. West. "Far-infrared generation by doubly resonant difference frequency mixing in a coupled quantum well two-dimensional electron gas system". *Appl. Phys. Lett.*, 65(4):445–447, 1994.

[6] J. V. D. Veliadis, J. B. Khurgin, and Y. J. Ding. "Engineering of the nonradiative transition rates in modulation-doped multiple-quantum wells". *IEEE J. Quantum Electronics*, 32(7):1155–1160, 1996.

[7] Jurgen H. Smet, Clifton G. Fonstad, and Qing Hu. "Intrawell and interqwell intersubband transitions in multiple quantum wells for far-infrared sources". *J. Appl. Phys.*, 79(12):9305–9320, 1996.

[8] A. Afzali-Kushaa, G. I. Haddad, and T. B. Norris. "Optical pumped intersubband lasers based on quantum wells". *IEEE J. Quantum Electron*, 31(1):135–143, 1995.

[9] F. H. Julien, A. Saár, J. Wang, and J. P. Leburton. "Optically pumped intersub-band emission in quantum wells". *Electronics Letters*, 31(10):838–839, 1995.

[10] F. H. Julien, Z. Moussa, P. Boucaud, Y. Lavon, A. Saár, J. Wang, J. P. Leburton, V. Berger, J. Nagle, and R. Planel. "Intersubband mid-infrared emission in optically pumped quantum wells". *Superlattices and Microstructures*, 19(1):69–79, 1996.

[11] Y. Lavon, A. Saár, Z. Moussa, F. H. Julien, and R. Planel. "Intersubband transitions from the second subband in a coupled quantum wells structure". *Superlattices and Microstructures*, 19(1):1–7, 1996.

[12] Y. Lavon, A. Saár, Z. Moussa, F. H. Julien, and R. Planel. "Observation of optically pumped midinfrared intersubband luminnescence in a coupled quantum wells structure". *Appl. Phys. Lett.*, 67(14):1984–1986, 1995.

[13] C. Y. Sung, T. B. Norris, A. Afzali-Kushaa, and G. I. Haddad. "Femtosecond intersubband relaxation and population inversion in stepped quantum well". *Appl. Phys. Lett.*, 68(4):435–437, 1996.

[14] Shmuel I. Borenstain and Joseph Katz. "Evaluation of the feasibility of a far-infrared laser based on intersubband transitions in GaAs quantum well". *Appl. Phys. Lett.*, 55(7):654–656, 1989.

[15] Z. Xin and H. N. Rutt. "Effect of inhomogenity on quantum well far-infrared lasers". *J. Appl. Phys.*, 83(3):1491–1495, 1998.

[16] R. Grey. Private communications, 1997.